



Published in final edited form as:

Oncogene. 2015 February 26; 34(9): 1126–1140. doi:10.1038/onc.2014.37.

The *WIP1* Oncogene Promotes Progression and Invasion of Aggressive Medulloblastoma Variants

Meghan C. Buss¹, Marc Remke⁴, Juhyun Lee¹, Khanjan Gandhi³, Matthew J. Schniederjan^{2,3}, Marcel Kool⁵, Paul A. Northcott⁵, Stefan M. Pfister^{5,6}, Michael D. Taylor⁴, and Robert C. Castellino^{1,2,3}

¹Department of Pediatrics, Aflac Cancer and Blood Disorders Center, Atlanta, GA, USA

²Children's Healthcare of Atlanta, Atlanta, GA, USA

³Winship Cancer Institute, Emory University School of Medicine, Atlanta, GA, USA

⁴Division of Neurosurgery, Arthur and Sonia Labatt Brain Tumour Research Center, and Program in Developmental and Stem Cell Biology, The Hospital for Sick Children, University of Toronto, Toronto, Ontario, Canada

⁵German Cancer Research Center, Heidelberg University Hospital, Heidelberg, Germany

⁶Department of Pediatric Hematology, Oncology and Immunology, Heidelberg University Hospital, Heidelberg, Germany

Abstract

Recent studies suggest that medulloblastoma, the most common malignant brain tumor of childhood, is comprised of four disease variants. The *WIP1* oncogene is overexpressed in Group 3 and 4 tumors, which contain medulloblastomas with the most aggressive clinical behavior. Our data demonstrate increased *WIP1* expression in metastatic medulloblastomas, and inferior progression-free and overall survival of patients with *WIP1* high-expressing medulloblastoma. Microarray analysis identified up-regulation of genes involved in tumor metastasis, including the G protein-coupled receptor CXCR4, in medulloblastoma cells with high *WIP1* expression. Stimulation with the CXCR4 ligand SDF1 α activated PI-3 kinase signaling, and promoted growth and invasion of *WIP1* high-expressing medulloblastoma cells in a *p53*-dependent manner. When xenografted into the cerebellum of immunodeficient mice, medulloblastoma cells with stable or endogenous high *WIP1* expression exhibited strong expression of CXCR4 and activated AKT in primary and invasive tumor cells. *WIP1* or *CXCR4* knock-down inhibited medulloblastoma growth and invasion. *WIP1* knock-down also improved the survival of mice xenografted with *WIP1* high-expressing medulloblastoma cells. *WIP1* knock-down inhibited cell surface localization of CXCR4 by suppressing expression of the G protein receptor kinase 5, *GRK5*. Restoration of wild-type *GRK5* promoted Ser339 phosphorylation of CXCR4 and inhibited the

Users may view, print, copy, and download text and data-mine the content in such documents, for the purposes of academic research, subject always to the full Conditions of use:http://www.nature.com/authors/editorial_policies/license.html#terms

Corresponding Author: Robert C. Castellino, HSRB, 1760 Haygood Drive, N.E., Room E394, Atlanta, GA 30322. Telephone: (404) 727-2078. Fax: (404) 727-4455. rccaste@emory.edu.

Conflict of Interest: Dr. Castellino's and Dr. Taylor's work has been funded by the NIH. Other authors declare no conflict of interest.

growth of *WIP1*-stable medulloblastoma cells. Conversely, *GRK5* knock-down inhibited Ser339 phosphorylation of *CXCR4*, increased cell surface localization of *CXCR4*, and promoted the growth of medulloblastoma cells with low *WIP1* expression. These results demonstrate cross-talk among *WIP1*, *CXCR4*, and *GRK5*, which may be important for the aggressive phenotype of a subclass of medulloblastomas in children.

Keywords

medulloblastoma; *WIP1*; *PPM1D*; *CXCR4*; *GRK5*

Introduction

Advances in neurosurgical techniques, combination chemotherapy, cranio-spinal radiation, and supportive care measures have led to dramatic overall improvements in survival from medulloblastoma.^{1,2} Yet, most survivors suffer long-term toxicities³⁻⁵, and up to one-third may develop recurrent disease.^{6,7} Improvements in treatment will likely require a better understanding of the molecular pathobiology of this disease. To that end, recent gene expression analyses suggest that medulloblastoma consists of 4 disease variants: *WNT*, *SHH*, Group 3, and Group 4.^{8,9}

Approximately 10% of medulloblastomas demonstrate active *Wingless (WNT)* signaling. These tumors exhibit classic histology, cytogenetics with monosomy of chromosome 6, and mutations of *CTNNB1* and *DDX3X* in 50-85% of cases.¹⁰ Retrospective studies suggest that the 5-year progression-free (PFS) and overall survival (OS) of patients with *WNT*-activated medulloblastoma is > 90%.^{9,11} Future clinical trials will likely reduce treatment intensity to prevent therapy-related toxicities.

Thirty percent of medulloblastomas exhibit active *Sonic Hedgehog (SHH)* signaling. These tumors display classic or nodular/desmoplastic histology, 9q deletion in 50% of cases^{9,12}, and positive immunohistochemistry (IHC) for *SFRP1*¹² or *GAB1*¹³. Studies suggest that upregulation of *CXCR4* and mutation of the key tumor suppressor, *p53*, represent distinct subgroups within *SHH* medulloblastomas.^{14,15} The 5-year OS of children > 3 years-old with *SHH*-activated medulloblastomas is 68%.⁹ Attempts to salvage those patients with progressive disease with a targeted *SHH* inhibitor have yielded mostly transient responses.^{16,17} This suggests a need for combinations of *SHH*- and other molecularly-targeted therapies to avoid treatment resistance.

The biology of Group 3 and 4 medulloblastomas is less-well understood. There are currently no viable targeted treatments for these medulloblastoma variants. *MYC* amplification¹⁸ and a *MYC* target gene expression signature¹⁹ constitute hallmark oncogenic features of Group 3 tumors, which contain a high percentage of large or anaplastic cells, and a dismal 39% 10-year OS.⁹ Both Group 3 and 4 medulloblastomas have an increased incidence of clinically-relevant, poor prognostic features, including chromosome i17q by cytogenetics and metastasis at diagnosis.^{13,20}

WIP1, on chromosome 17q22-q23, inhibits p53 activity and functions as an oncogene when expressed at high levels along with oncogenes, including *Myc*.²¹⁻²³ *WIP1* amplification or overexpression has been described in multiple cancers that are *wild-type* for *p53*.^{21,23,24} We and others have described amplification and overexpression of *WIP1* in 64% of human medulloblastomas.^{18,25,26} We recently reported increased *WIP1* expression in Group 3 and 4 medulloblastomas.²⁷

We now demonstrate increased *WIP1* expression in metastatic medulloblastomas, and inferior survival in patients with *WIP1* high-expressing medulloblastoma. Gene expression demonstrated up-regulation of *CXCR4* in *WIP1* high-expressing medulloblastomas. *CXCR4* activation promoted AKT phosphorylation, increased growth, and invasion of *WIP1*-stable medulloblastoma cells *in vitro* and in mouse models. *WIP1* or *CXCR4* knock-down inhibited AKT activation, growth, and migration of *WIP1* high-expressing medulloblastoma cells. *WIP1* knock-down inhibited cell membrane localization of *CXCR4* due to suppression of the G protein receptor kinase 5, *GRK5*. Restoration of wild-type *GRK5* promoted Ser339 phosphorylation of *CXCR4* and inhibited the growth of *WIP1* stable cells. Conversely, *GRK5* knock-down in cells with low *WIP1* expression inhibited *CXCR4* phosphorylation, increased cell membrane expression of *CXCR4*, and promoted medulloblastoma growth. This suggests an important cross-talk among *WIP1*, *CXCR4*, and *GRK5*, which promotes tumor growth and invasion, and which may be responsible for the aggressive behavior of *WIP1* high-expressing medulloblastomas.

Results

We validated increased *WIP1* expression in a cohort of 64 medulloblastomas with gain of chromosome 17q, and in Group 3 and 4 medulloblastomas (Fig. 1A-B). Patient characteristics are shown in Table 1. We noted a significant association between high *WIP1* expression and medulloblastomas classified as Chang stage M2-3, due to dissemination of medulloblastoma cells beyond the primary site (Fig. 1C). One patient did not have information available regarding Chang staging. Further analysis demonstrated inferior PFS and OS of patients with *WIP1* high-expressing medulloblastomas (Fig. 1D-E).

Since high *MYC* expression or amplification has been identified as a defining characteristic of Group 3 medulloblastomas^{8,18,19,28}, we used *MYC* high-expressing D556, D425, and Med8A cells to model aggressive medulloblastoma variants.^{18,29} We have previously described high *WIP1* expression in Group 3 and 4 human medulloblastomas, and in D425 and Med8A cells.²⁷ In addition, we have shown that stable expression of *WIP1* in D556 cells significantly enhances medulloblastoma growth.²⁷ By Western blotting, we also found increased expression of the Group 3 and 4 markers, *NPR3* and *KCNA1*³⁰, in D556-*WIP1* stable clones (Supplementary Fig. S1).

Principal component analysis showed a clear separation in gene expression among D556 cells with stable expression of wild-type *WIP1*, empty vector, or mutant, phosphatase-deficient *WIP1*.²⁷ Pathway analysis revealed up-regulation of genes involved in cell adhesion and migration in D556 *WIP1*-stable cells, including the G protein-coupled receptor *CXCR4*. Conversely, the gene for adenylate cyclase 1, *ADCY1*, was down-regulated in

D556-*WIP1* stable cells (Fig. 2A & S2). Others have shown that CXCR4 activation inhibits adenylate cyclase, which, in turn, reduces intracellular cAMP to promote growth of brain tumor cells.³¹ By real-time, RT-PCR, we confirmed increased *CXCR4* in medulloblastoma cells with stable or endogenous high *WIP1* expression (Fig. 2B). Western blotting and immunofluorescence (IF) confirmed increased CXCR4 protein expression in D556 *WIP1*-stable cells (Fig. 2C-D). Thus, high *WIP1* expression correlated with up-regulation of CXCR4 in cell line models of aggressive medulloblastoma variants.

To determine the functional significance of increased CXCR4 expression, we serum-starved and stimulated D556-*WIP1* clones with the CXCR4 ligand, CXCL12 (SDF1 α). Only D556-*WIP1* stable cells proliferated in response to SDF1 α stimulation (Fig. 3A & S3A-B). Since SDF1 α stimulation is known to activate downstream PI-3 kinase pathways, we examined phosphorylation of Ser473 on the PI-3 kinase target, AKT. Western blotting demonstrated increased baseline and SDF1 α -stimulated phosphorylation of AKT in D556-*WIP1* cells (Fig. 3B). Similarly, SDF1 α increased Ser473 phosphorylation of AKT and increased growth of endogenous *WIP1* high-expressing D425 (Fig. 3C-E & S3C) and Med8A (Fig. 3F-H & S3C) cells.

To examine the dependence of CXCR4 activity on *WIP1*, we transduced D556 and D425 cells with negative control or *WIP1* shRNA. SDF1 α stimulation enhanced the viability of D556-*WIP1*, but not D556-pcDNA or D556-*WIP1* D314 stable cells in serum-free conditions (*, Fig. 4A-C). *WIP1* knock-down inhibited the growth of D556-*WIP1* stable cells by almost 50% (**, Fig. 4A-B). *WIP1* knock-down also significantly inhibited the proliferative effect of SDF1 α stimulation in D556-*WIP1* stable cells (***, Fig. 4A-C). We observed similar effects in D425 cells, which have endogenous high *WIP1* expression (Fig. 4D-E).

Ser339-phosphorylation has previously been implicated in activation of CXCR4 and downstream activation of PI-3 kinase signaling.³² *WIP1* knock-down did not change expression of total CXCR4. However, *WIP1* knock-down increased Ser339 CXCR4 phosphorylation in the cytoplasmic fraction of D556 cells with stable expression of wild-type *WIP1* (Supplementary Fig. S4A). *WIP1* knock-down also increased Ser339 phosphorylation of CXCR4 (Supplementary Fig. S4B) and inhibited Ser473 phosphorylation of AKT in D425 cells (Fig. 4F). In two different D556-*WIP1* stable clones, *WIP1* knock-down inhibited membrane expression of CXCR4 (Supplementary Fig. S5). Thus, *WIP1* knock-down altered CXCR4 localization, inhibited downstream phosphorylation of AKT, and prevented the growth-promoting effects of SDF1 α in *WIP1* high-expressing medulloblastoma cells.

Since CXCR4 signaling has previously been implicated in invasion and metastasis, we examined invasion and migration of D556 stable clones *in vitro*. Neither D556-pcDNA nor D556-*WIP1* D314A stable clones exhibited significant invasion. In contrast, D556-*WIP1* stable clones demonstrated significant invasion through Boyden chambers that contain SDF1 α as a chemo-attractant (*, Fig. 5A-B). *WIP1* knock-down inhibited the ability of D556-*WIP1* stable clones to invade through chambers exposed to SDF1 α . We also monitored cell migration in real time. In the presence of SDF1 α , D556-*WIP1* stable cells

demonstrated increased migration, as quantified by the rate of change of the cell index (CI)²⁷. The CI slope was significantly higher in migration chambers containing D556-*WIP1* cells and SDF1 α (Fig. 5C-D). This suggests that high *WIP1* expression facilitates medulloblastoma migration and invasion.

Since most of the functions of *WIP1* that have been described to date have required functional *p53*, we examined the *p53* dependence of the interaction between *WIP1* and CXCR4. As we have previously demonstrated, stimulation with SDF1 α increased the number of viable D556-*WIP1*, but not D556-pcDNA, stable cells (Fig. 3). *p53* knockdown did not affect the viability of unstimulated or SDF1 α -stimulated D556-pcDNA cells (Supplementary Fig. S6A). However, *p53* knockdown resulted in reduced serine 473 (Ser473) phosphorylation of AKT (Supplementary Fig. S6B) and inhibited the increase in viability of D556-*WIP1* cells following SDF1 α stimulation that was seen in D556-*WIP1* cells transfected with scrambled, negative control siRNA (Supplementary Fig. S6A). We also examined *p53* dependence of the interaction between *WIP1* and CXCR4 on invasion using the previously characterized *p53* mutant, *WIP1* high-expressing Daoy cell line.²⁷ Unlike D556-*WIP1* stable clones, which demonstrated a significant increase in invasion compared to D556 cells with stable expression of an empty vector (Fig. 5), neither Daoy-pcDNA nor Daoy-*WIP1* stable cells differed in the number of cells that invaded through a Matrigel Invasion Chamber when attracted with the chemokine SDF1 α (Supplementary Fig. S7).

We further validated this *p53* dependence by treating D556-pcDNA and D556-*WIP1* stable cells with the small molecule inhibitors of *p53* function, Nutlin-3a and RITA. Nutlin-3a is a *cis*-imidazoline analog that bind with high affinity to the endogenous *p53* inhibitor HDM2. It inhibits the interaction between HDM2 and *p53*, which stabilizes *p53* and promotes apoptosis or senescence of cancer cells that contain wild-type *p53*.^{33,34} The small molecule RITA binds with high affinity to the amino-terminal domain of *p53*.³⁵ This results in activation of *p53*, transcriptional repression of anti-apoptotic proteins, such as Bcl-2 and survivin, and downregulation of oncogenic signaling pathways, including MYC and AKT.^{36,37} Treatment with Nutlin-3a or RITA did not affect the viability of unstimulated or SDF1 α -stimulated D556-pcDNA cells (Supplementary Fig. S6C, E). However, treatment with Nutlin-3a resulted in reduced serine 473 (Ser473) phosphorylation of AKT (Supplementary Fig. S6D). Treatment with either Nutlin-3a or RITA also inhibited the increase in viability of D556-*WIP1* cells following SDF1 α stimulation that was seen in vehicle-treated D556-*WIP1* cells (Supplementary Fig. S6C, E). Thus, either *p53* knockdown, presence of mutant *p53*, or treatment with the small molecule *p53*-inhibiting drugs Nutlin-3a or RITA suppressed SDF1 α -stimulated growth and migration of *WIP1* high-expressing medulloblastoma cells. This suggests that the interaction between CXCR4 and *WIP1* signaling is dependent on the presence of functional *p53*.

We have previously demonstrated increased tumor cell proliferation and reduced overall survival of mice bearing intra-cerebellar xenografts of D556-*WIP1* stable cells, compared to mice bearing D556-pcDNA stable cells.²⁷ By H&E staining, 7 of 9 D556-*WIP1* xenografts showed evidence of local or distant brain metastasis (Fig. 6A). Neither parental (n = 2), nor D556-pcDNA (n = 9) xenografts, showed evidence of dissemination. By IHC, we identified

increased cytoplasmic and membrane expression of CXCR4 and its downstream target, Ser473-phosphorylated AKT, in D556-*WIP1* xenografted primary and metastatic cells (Fig. 6A-B).

To confirm dissemination of xenografts, we examined 10 consecutive sagittal sections, with 10 mm spacing between sections, of each tumor for H&E staining and immunoreactivity against CXCR4 and phospho-AKT (Ser473). Phospho-AKT (Ser473) was expressed diffusely in all tumor cells and was moderate to strong in intensity in all D556-*WIP1* xenografts (Table 2). At best, IHC for phospho-AKT (Ser473) was focal and weak (1+, <10%; Supplementary Fig. S8) in D556-pcDNA xenografts. In addition, D556-*WIP1* xenografts had unequivocal evidence of invasion, almost exclusively as infiltration down the perivascular space (Supplementary Fig. S9). This is a pattern of tumor dissemination that is frequently observed in invasive human medulloblastomas. One D556-*WIP1* xenograft had clear evidence of leptomeningeal metastasis out to the rostral cortex and olfactory bulb, which then invaded into the cortex along blood vessels. No such distant or local metastases were present in D556-pcDNA xenografted tumors.

We next confirmed this finding using intracerebellar xenografts of endogenous *WIP1* high-expressing D425 cells, infected with control or *WIP1* shRNA. Fluorescence microscopy of fresh sagittal brain sections from symptomatic animals xenografted with D425 cells infected with control lentivirus demonstrated GFP fluorescence both in the cerebellum, at the site of xenografting, and along the leptomeninges (Fig. 6C). A similar pattern of dissemination is often seen by MRI in children with metastatic medulloblastoma. As with D556-*WIP1* stable xenografts, mice xenografted with D425 cells developed primary and metastatic tumors, both of which demonstrated positive cytoplasmic staining for CXCR4 and Ser473-phosphorylated AKT (Fig. 6E). In contrast, mice xenografted with *WIP1* shRNA-infected D425 cells demonstrated significantly improved survival (Fig. 6D). Interestingly, tumors from sh*WIP1*-infected D425 cells exhibited staining for CXCR4 that was predominantly nuclear. And, staining for Ser473-phosphorylated AKT was virtually absent in these tumors (Fig. 6E). These observations support our *in vitro* findings of increased CXCR4 and PI-3 kinase signaling in *WIP1* high-expressing medulloblastomas. In fact, Wu *et al.* recently showed that PI-3 kinase signaling is a crucial driver of leptomeningeal dissemination of *SHH* medulloblastomas.³⁸

To confirm the interaction between *WIP1* and CXCR4, we knocked-down *CXCR4*. Infection of medulloblastoma cells with *CXCR4* shRNA resulted in a 70% reduction in *CXCR4* expression (Fig. 7C) and a 40% reduction in viable D556-*WIP1* cells (Fig. 7A-B). In serum-free conditions, *CXCR4* knock-down inhibited the growth of SDF1 α -stimulated D556-*WIP1* cells by 60% (**, Fig. 7D). *CXCR4* knock-down did not affect the viability of D556 cells with stable expression of a phosphatase-dead *WIP1*. By Western blotting, *CXCR4* knock-down resulted in an 80% reduction in Ser473 phosphorylation of AKT in D556-*WIP1*, but not in *WIP1* mutant D556-*WIP1* D314A stable cells (Fig. 7C).

We validated the results of *CXCR4* knock-down using the small molecule CXCR4 inhibitor, AMD3100. Alone, AMD3100 did not affect cell viability. However, similar to the effects of *CXCR4* knock-down, AMD3100 prevented the effects of SDF1 α stimulation on growth of

D556-*WIP1* stable cells. (Fig. 7E-F). Western blotting confirmed inhibition of Ser473 AKT phosphorylation in D556-*WIP1* cells treated with AM3100 and stimulated with SDF1 α (Fig. 7G).

Since *WIP1* knock-down failed to alter total CXCR4 expression, but did affect CXCR4 localization *in vitro* as well as in intra-cerebellar xenografts, we examined the role of G-protein receptor kinases in trafficking of CXCR4. Others have shown that the G-protein receptor kinase 5, GRK5, promotes CXCR4 phosphorylation and internalization.³⁹ Our analysis suggests a high degree of co-regulated expression of *WIP1* and *GRK5* in our cohort of human medulloblastomas ($R = 0.44$, $p < 0.005$). Our microarray data demonstrated significant down-regulation of *GRK5* in D556-*WIP1* stable clones. By real-time, RT-PCR and Western blotting, we validated significantly lower levels of *GRK5* mRNA and protein in D556-*WIP1* stable clones (Fig. 8A-B). Reduced GRK5 levels corresponded with reduced Ser339-phosphorylated CXCR4 in D556-*WIP1* stable clones (Fig. 8B). To study the functional implications of altered GRK5 expression, we transfected expression plasmids containing an empty vector, wild-type, or kinase-dead *GRK5* (*GRK5* K215R) into D556-*WIP1* or D556-*WIP1* D314A stable cells. Neither wild-type nor kinase-dead *GRK5* had a significant effect on the growth of D556 cells that stably express phosphatase-dead *WIP1*. However, transfection with wild-type *GRK5* reduced the number of viable D556-*WIP1* stable cells by 50% (Fig. 8C-D). Transfection of kinase-dead *GRK5* also inhibited the growth of D556-*WIP1* stable cells, but to a lesser degree. Western blotting revealed an increase in Ser339 CXCR4 phosphorylation, in *GRK5*-transfected D556-*WIP1* cells (Fig. 8E). There was no difference in Ser339-phosphorylated CXCR4 in D556-*WIP1* D314A stable cells following transfection with empty vector, wild-type, or kinase-dead *GRK5*. Moreover, *GRK5* transfection rescued D556-*WIP1* cells from the effects of *GRK5* knock down. *GRK5* knock down reduced Ser339 phosphorylation of CXCR4 in D556-*WIP1* stable cells transfected wild-type *GRK5*, and increased the number of viable D556-*WIP1* stable cells to near baseline levels (Supplementary Fig. S10). Thus, GRK5 may suppress the growth of *WIP1* high-expressing medulloblastoma cells by promoting Ser339 phosphorylation of CXCR4.

We also examined the role of CXCR4 phosphorylation at serine 339 in D425 medulloblastoma cells, which have high endogenous *WIP1* expression. The HA-tagged *CXCR4-S339A* lentivirus expresses a mutant CXCR4 in which serine has been mutated to alanine at amino acid 339. This results in a form of CXCR4 that is resistant to phosphorylation at serine 339. Infection of D425 cells with HA-tagged *CXCR4-S339A* lentivirus inhibited cell viability and responsiveness to SDF1 α stimulation. Co-infection of D425 cells with *WIP1* shRNA and HA-tagged *CXCR4-S339A* further suppressed cell viability and also inhibited responsiveness to SDF1 α stimulation (Supplementary Fig. S11). This suggests that phosphorylation of serine 339 on CXCR4 is important for cell viability. We have shown that activation of CXCR4 induces signaling AKT, which promotes cell growth. What is not clear from this experiment is the localization of mutant CXCR4-S339A protein. It is possible that the mutant protein is not being expressed at the plasma membrane, which would explain the reduced cell viability and lack of response to SDF1 α stimulation.

To determine if *GRK5* knock-down could recapitulate the proliferative effects of increased *WIP1* expression, we infected D556-pcDNA and D556-*WIP1* stable cells with empty vector, negative control or *GRK5* shRNA-encoding lentivirus. *GRK5* knock-down resulted in a 50% reduction in expression of *GRK5* mRNA or protein (Fig. 8G & S12), and a corresponding increase in the viability of empty vector-containing D556 cells (Fig. 8F). *GRK5* knock-down did not significantly affect the viability of D556-*WIP1* stable cells. Western blotting revealed reduced Ser339 phosphorylation of CXCR4 in sh*GRK5*-infected D556-pcDNA cells (Fig. 8G). Immunofluorescence validated increased CXCR4 expression and membrane localization following *GRK5* knock-down in D556-pcDNA stable cells (Supplementary Fig. S13). This suggests that *GRK5* promotes internalization of CXCR4. Conversely, *WIP1* suppresses *GRK5* expression, which in turn permits membrane localization of CXCR4 and medulloblastoma growth, and invasion in response to SDF1 α stimulation (Fig. 8H). Thus, strategies that inhibit CXCR4 or promote *GRK5* expression may be useful, especially in the treatment of *WIP1* high-expressing medulloblastomas.

Discussion

A number of retrospective studies suggest a prognostic relevance for genes on chromosome 17q in medulloblastoma.⁴⁰⁻⁴³ Group 3 and 4 medulloblastomas exhibit an increased frequency of chromosome 17 alterations and increased expression of *WIP1*.^{9,12,20} In a multivariate analysis, either loss of chromosome 17p or gain of 17q was prognostic of poor OS.⁹ One publication suggests a role for the chromosome 17q gene *LIM and SH3 protein 1 (LASP1)* in medulloblastoma metastasis.⁴⁴ We have now identified an association between high *WIP1* expression and inferior PFS and OS in medulloblastoma. We have also identified significantly higher *WIP1* expression in metastatic Chang-stage M2-3 medulloblastomas.

Metastatic disease at diagnosis has long been considered a poor prognostic factor in medulloblastoma. Recent studies report an overall frequency of medulloblastoma metastasis (M+) of 24%. M+ disease is least common in *WNT*-activated (0-18%) and most common in Group 3 (30-75%) and 4 (30-31%) tumors.^{9,12,20} Kaplan-Meier analysis demonstrates significantly worse OS in children > 3 years of age and in group 4 tumors with M+ disease.⁹ Sadly, the mechanisms that drive medulloblastoma invasion and metastasis remain poorly understood.

WIP1, located on chromosome 17q22-23, is a PP2C-like serine/threonine protein phosphatase that is a direct target of the tumor suppressor, p53.⁴⁵ It, in turn, regulates the cell cycle through p53-dependent mechanisms. *WIP1* directly dephosphorylates and inactivates p53 at Ser15. It also inactivates important regulators of p53 function, dephosphorylating p38MAPK at Thr180⁴⁶ and MDM2 at Ser395.⁴⁷ Upstream of p53, *WIP1* inactivates an early step in DNA-damage response by dephosphorylating the ataxia-telangiectasia mutated (ATM) kinase on Ser1981.⁴⁸ *WIP1* also binds and dephosphorylates the serine/threonine kinase, Chk1, at Ser345.⁴⁹ And, it inactivates Chk2 at Thr68.^{50,51} p53-independent *WIP1* regulatory roles are not as well characterized, but *WIP1* is thought to play an important role, independent of p53, in the maintenance of mouse intestinal stem cells⁵² and, with hedgehog signaling, in the growth of human cancer cell lines.⁵³

Wip1 is best understood for its important role in DNA damage response and tumorigenesis. While evidence from mouse models suggests that *Wip1* overexpression alone is insufficient for cancer formation, *Wip1* can cooperate with other “classic” oncogenes to transform mouse embryo fibroblasts.⁵⁴ *WIP1* amplification or overexpression has been described in multiple cancers that are *wild-type* for *p53*.^{21,23,24} Recent publications have reported activating mutations in the C-terminus of *WIP1* in some cancers.⁵⁵⁻⁵⁷ However, to date, there have been no reports implicating *WIP1* in cancer invasion or metastasis.

G protein-coupled receptors have been implicated both in brain development and cancer metastasis.⁵⁸ CXCR4 and its ligand, SDF1 α , are required for appropriate cerebellar development.⁵⁹ CXCR4 is also the most common chemokine receptor expressed on cancer cells, and promotes cancer growth and metastasis.⁶⁰ Other groups have shown that increased CXCR4 expression in primary CNS malignancies, including medulloblastoma, is associated with inferior survival.^{15,31,61,62} Sengupta *et al.* reported high CXCR4 expression in infant and adult medulloblastomas with classic or desmoplastic histology. SHH activation promoted cell surface accumulation of CXCR4, increased downstream signaling, and cell growth in culture.¹⁵

Using human cell line models of aggressive medulloblastoma variants, with increased expression of *MYC* and either stable or endogenous high *WIP1* expression, we identified increased expression of CXCR4 and activation of downstream targets of PI-3 kinase signaling in response to SDF1 α stimulation. We observed increased growth and invasion of *WIP1*-stable medulloblastoma cells *in vitro* and in orthotopic, xenografted mouse models. *WIP1* high-expressing xenografts demonstrated invasion as well as local and distant metastases, which stained strongly for CXCR4 and Ser473-phosphorylated AKT. Conversely, *WIP1* or *CXCR4* knock-down inhibited the effects of SDF1 α on PI-3 kinase signaling, growth, and migration. SCID mice xenografted with sh*WIP1*-infected D425 cells demonstrated increased survival. This suggests an important interaction between *WIP1* and *CXCR4* which promotes growth and dissemination of aggressive medulloblastoma variants.

G protein-coupled receptors (GPCRs) are regulated by desensitization, internalization, and degradation. This process is initiated by G protein-coupled receptor kinases (GRKs), which phosphorylate serine or threonine residues in the cytoplasmic tail following GPCR activation.⁶³ Woerner *et al.* showed that SDF1 α stimulation promotes Ser339 phosphorylation of CXCR4 in human astrocytomas.³² Others have shown that mutation of Ser338 and Ser339 results in reduced SDF1 α -stimulated phosphorylation of these sites.⁶⁴ GRK5 phosphorylation of Hsp70 interacting protein promotes internalization of CXCR4.³⁹ We found that D556-*WIP1* cells had reduced levels of *GRK5*. Transfection of *GRK5* into D556-*WIP1* cells increased Ser339 phosphorylation of CXCR4 and reduced proliferation. Conversely, knock-down of *GRK5* resulted in reduced Ser339 phosphorylation of CXCR4 and increased proliferation of D556 containing an empty vector. Thus, modulation of *GRK5* expression is an important mechanism through which *WIP1* alters phosphorylation and function of CXCR4 to promote medulloblastoma growth and dissemination.

Using mouse models, Wu *et al.* recently demonstrated mechanisms of metastasis by inserting the Sleeping Beauty (SB) transposon into *Patched* +/- mice. Dysregulation of *Shh*

signaling in granule neuron precursor (GNP) cells leads to medulloblastoma that is localized to the cerebellum in 15-39% of *Patched* +/- mice.^{38,65,66} Expression of SB transposase from the *Math1* promoter resulted in 97% of *Patched* +/- mice with metastatic medulloblastoma by 10 weeks of age. Interestingly, PI-3 kinase signaling was a significant driver of leptomeningeal dissemination in *Shh*-activated, *Patched* +/-/*Math1*-*SB11*/T2Onc mouse medulloblastomas.³⁸

Mumert *et al.* used the RCAS/*tv-a* system in cerebellar neural progenitor cells to validate candidate genes (*Eras*, *Lhx1*, *Ccrk*, and *Akt*) identified by Wu *et al.* The incidence of spinal metastases was most significant in mice with co-expression of *Shh* and either *Ccrk* or *Akt*.⁶⁷ It is possible that *Eras*, *Lhx1*, *Ccrk*, and *Akt* are of greatest significance in *SHH*-activated human medulloblastomas while genes on chromosome 17q, such as *WIP1*, have a more significant role in dissemination of non-*SHH*-activated medulloblastomas.

Materials and Methods

Materials

SDF1 α (CXCL12) (PeproTech, Rocky Hill, NJ) was prepared in H₂O and used at 0.1-1 μ g/mL. AMD3100 (Sigma-Aldrich, St. Louis, MO) was prepared in H₂O and diluted in media to 20 μ M. Nutlin 3A/B (Cayman Chemical Company, Ann Arbor, MI) was prepared in EtOH at a stock concentration of 3200 μ M and used at a concentration of 8 μ M (4 μ M effective). RITA (Selleck Chemicals, Houston, TX) was prepared in DMSO at a stock concentration of 50 μ M and was diluted in media to 25nM for experiments.

Cell Culture

D556, Med8A, and D425 cell lines, and D556 stable clones were derived and maintained as previously described.²⁷

Proliferation Assays

2×10^4 cells were plated in 96-well plates, serum-starved, and cultured in phenol red-free MEM media (Mediatech, Inc., Manassas, VA). For knockdown, cells were infected with control or sh*WIP1* lentivirus during starvation, and treated with vehicle or 1 μ g/mL SDF1 α . 48 hours post-treatment, WST-1 (Roche Applied Science, Indianapolis, IN) was added at a 1:100 dilution, or an equal volume of Cell Titer-Glo (Promega, Madison, WI). For WST-1 assays, plates were analyzed using a Synergy MX plate reader (wavelength-450nm/reference-620nm; BioTek, Winooski, VT). For Cell Titer-Glo assays, luminescence was measured using a 1 second integration time. Alternatively, the number of viable cells in an experiment was counted by trypan blue exclusion, using standard methods.

Gene Expression Microarray Analysis

Patients were partitioned using median *WIP1* expression as a cutoff. Survival was measured from diagnosis until death or last follow-up. Patient survival was analyzed according to the Kaplan-Meier method, using log-rank statistics. Copy number status of chromosome 17q was determined using array-based comparative genomic hybridization (CGH), as previously published. Gene expression profiling data were performed and analyzed as previously

described.^{28,68} Using R2 software (<http://r2.amc.nl>), we compared *WIP1* expression patterns according to 17q status, subgroup, and M-stage, as previously described.^{28,68} Subgroup affiliation was determined using unsupervised clustering approaches.^{28,68}

Quantitative Real-Time, RT-PCR

Total cellular RNA was extracted, as previously described.²⁷ Quantitative real-time, RT-PCR reactions containing cDNA, Syber Green PCR Master Mix (Life Technologies, Grand Island, NY) and primers for human *WIP1*, *CXCR4*, *GRK5*, and/or *Glyceraldehyde-3 Phosphate Dehydrogenase (GAPDH)* were run on an ABI 7500 Real-Time PCR Cycler (Life Technologies), using absolute quantification with a standard curve. Primer sequences are available upon request. Amplification products were verified by analysis of melting curves. Serial cDNA dilutions were used to determine standard curves for each primer. Analysis of housekeeping gene expression was included with each run. Absolute gene expression was determined based on standard curves. Target gene expression was normalized to *GAPDH* expression.

Western Blotting

Protein was extracted, quantified, and probed with antibody, as previously described.⁶⁹ Whole cell lysates were extracted using RIPA buffer (Cell Signaling). Nuclear and cytoplasmic lysates were extracted using the NE-PER Nuclear and Cytoplasmic Extraction Kit, according to the manufacturer (Thermo Scientific). Antibodies included AKT (Cell Signaling, Danvers, MA), phospho-AKT (S473) (Cell Signaling), CXCR4 (Abcam, Cambridge, MA), phospho-CXCR4 (S339) (Abcam), eEF2 (Cell Signaling), GRK4-6 (EMD Millipore, Billerica, MA), GRK5 (C-20) (Santa Cruz Biotechnology, Inc., Santa Cruz, CA), KCNA1 (Abcam), Lamin B1 (Cell Signaling), NPR3 (Abcam), WIP1 (Bethyl, Montgomery, TX), and β -actin (Sigma-Aldrich, St. Louis, MO). Secondary antibodies Alexa Fluor 680 goat anti-mouse IgG (Life Technologies) or IRDye 800 goat anti-rabbit IgG (Rockland, Gilbertsville, PA) were used at a dilution of 1:5,000. Immunoblots were imaged and quantified, as previously described.²⁷

Immunofluorescence

Cells were plated at 3.5×10^4 on Nunc Lab Tek Chamber Slides (Nalge Nunc, Rochester, NY), fixed with 4% paraformaldehyde, incubated with 50 mM NH_4Cl , and permeabilized with 0.3% Triton-X. To quench endogenous peroxidases, cells were incubated in 0.3% H_2O_2 in MeOH. Cells were subsequently incubated with 10% normal goat serum (Invitrogen) containing 0.3% Triton-X, blocked with 5% BSA, and incubated overnight at 4°C with primary antibody. Cells were then washed with TNT (1 mM Tris/HCl, 5 mM NaCl, 1% Tween-20) and incubated with goat, anti-rabbit Alexa Fluor 555 (Invitrogen) secondary antibody. Slides were mounted using Hard Set Mounting Media with DAPI (Vectashield, Vector Laboratories, Burlingame, CA). Images were acquired with an EVOS-fl fluorescent microscope (Advanced Microscopy Group, Bothell, WA).

SDF1 α Stimulation

Cells were plated at 1×10^5 - 1×10^6 in 6 well plates and either stimulated with 100 ng/mL SDF1 α (PeproTech) for 0, 2, 10 and 30 minutes, or with 1 μ g/mL SDF1 α for 48 hours in serum-free media.

Invasion Chamber Assays

Media containing 1 μ g/mL SDF1 α or vehicle was added to each well in a Matrigel Invasion Chamber (BD Biosciences, San Jose, CA), followed by placement of inserts. 2.5×10^4 cells were added to each insert and infected with lentivirus in the presence of 8 μ g/ μ l polybrene. Inserts were fixed in 100% methanol and stained with crystal violet.

Invasion Assays using xCelligence

Media containing vehicle or 1 μ g/mL SDF1 α was placed in the lower chambers of a CIM plate-16 (Roche Applied Science, Indianapolis, IN). 2×10^4 cells were seeded in the upper chamber of a CIM plate and monitored for real-time changes in cell index (CI). Error bars represent standard deviation. Slope of the CI was computed using RTCA Software.

Short Hairpin RNA Lentivirus Production and Infection

EGFP-tagged negative control and sh*WIP1* lentiviral expression constructs were gifts from Dr. Lawrence Donehower (Baylor College of Medicine).²⁷ psPAX2 and pVSVG plasmids were gifts from Dr. H. Trent Spencer (Emory University). The pLKO.1 empty vector control plasmid was a gift from Dr. Rita Nahta (Emory University). sh*CXCR4* and sh*GRK5* lentiviral expression constructs were purchased (Thermo Scientific). Production and infection with lentiviral particles were as previously described.²⁷

CXCR4 Inhibition Assays

1×10^5 cells were plated in 6 well plates, serum starved for 24 hours, and treated with vehicle, 100 ng/mL SDF1 α , and/or 20 μ M AMD3100. 48 hours post-treatment, cells were counted by trypan blue exclusion.

GRK5 Transfection

5×10^5 cells were plated in 6 well plates and, 24 hours later, were transfected with 1 μ g of pcDNA3, *GRK5*, or K215R *GRK5* plasmids (gifts from Dr. Jeffrey Benovic, Jefferson University) using Lipofectamine 2000 (Invitrogen), according to the manufacturer.

Mouse Handling

All mice were housed in an American Association of Laboratory Animal Care–accredited facility and were maintained in accordance with NIH guidelines. All animal care and experiments were approved by the Institutional Animal Care and Use Committee of Emory University (Protocol # DAR-2002073).

Xenografting of Medulloblastoma Cells

SCID mice were anesthetized and prepared, as described.²⁷ Mice were followed for symptoms and tissues processed, as described.²⁷

Tissue Handling and Immunohistochemistry

The brains of mice were excised in total, examined under a fluorescence stereomicroscope for evidence of GFP expression, sectioned sagittally down the midline, photographed for expression of GFP, and fixed in formalin. Tissue blocks were paraffin-embedded and cut into 5 mm sections. Antigen retrieval was performed by heating slides in sodium citrate for 20 minutes. After blocking endogenous peroxidases, slides were incubated with primary antibody. Secondary antibodies were applied according to the manufacturer (Vector Laboratories). Slides were stained with hematoxylin and mounted using VectaMount permanent mounting media (Vector Laboratories).

Statistical Analysis

Unless stated otherwise, all bar graphs display mean values of triplicate measurements. Error bars denote standard deviation (SD) among replicates. And, experiments were repeated at least three times with reproducible results. Results were analyzed using a two-tailed Student's t-test or one-way ANOVA in Microsoft Excel or Graphpad Prism 4 software to assess statistical significance. Values of $p < 0.05$ were considered statistically significant.

Supplementary Material

Refer to Web version on PubMed Central for supplementary material.

Acknowledgments

We thank Drs. Jeffrey Benovic, Lawrence Donehower, H. Trent Spencer, Laurent Brault, Jürg Schwaller, and Rita Nahta for gene expression constructs, Gregory Doho for assistance with analysis of microarrays, and Dr. Rita Nahta for editorial assistance. This work was supported by grants from the NIH (1R01CA172392-01, R.C.C.; CA159859, M.D. Taylor), St. Baldrick's Foundation (R.C.C.), CURE Childhood Cancer Foundation (R.C.C.), Southeastern Brain Tumor Foundation (R.C.C.), the Emory Egleston Children's Research Center (R.C.C.), and the Dr. Mildred-Scheel Foundation (M.R.).

References

1. McNeil DE, Cote TR, Clegg L, Rorke LB. Incidence and trends in pediatric malignancies medulloblastoma/primitive neuroectodermal tumor: a SEER update. *Surveillance Epidemiology and End Results. Med Pediatr Oncol.* 2002; 39:190–194. [PubMed: 12210449]
2. Gajjar A, Chintagumpala M, Ashley D, Kellie S, Kun LE, Merchant TE, et al. Risk-adapted craniospinal radiotherapy followed by high-dose chemotherapy and stem-cell rescue in children with newly diagnosed medulloblastoma (St Jude Medulloblastoma-96): long-term results from a prospective, multicentre trial. *Lancet Oncol.* 2006; 7:813–820. [PubMed: 17012043]
3. Dhall G. Medulloblastoma. *J Child Neurol.* 2009; 24:1418–1430. [PubMed: 19841429]
4. von Hoff K, Hinkes B, Gerber NU, Deinlein F, Mittler U, Urban C, et al. Long-term outcome and clinical prognostic factors in children with medulloblastoma treated in the prospective randomised multicentre trial HIT'91. *Eur J Cancer.* 2009; 45:1209–1217. [PubMed: 19250820]
5. Mabbott DJ, Spiegler BJ, Greenberg ML, Rutka JT, Hyder DJ, Bouffet E. Serial evaluation of academic and behavioral outcome after treatment with cranial radiation in childhood. *J Clin Oncol.* 2005; 23:2256–2263. [PubMed: 15800316]
6. Belza MG, Donaldson SS, Steinberg GK, Cox RS, Cogen PH. Medulloblastoma: freedom from relapse longer than 8 years--a therapeutic cure? *J Neurosurg.* 1991; 75:575–582. [PubMed: 1885975]

7. Torres CF, Rebsamen S, Silber JH, Sutton LN, Bilaniuk LT, Zimmerman RA, et al. Surveillance scanning of children with medulloblastoma. *N Engl J Med.* 1994; 330:892–895. [PubMed: 8114859]
8. Taylor MD, Northcott PA, Korshunov A, Remke M, Cho YJ, Clifford SC, et al. Molecular subgroups of medulloblastoma: the current consensus. *Acta Neuropathol.* 2012; 123:465–472. [PubMed: 22134537]
9. Kool M, Korshunov A, Remke M, Jones DT, Schlanstein M, Northcott PA, et al. Molecular subgroups of medulloblastoma: an international meta-analysis of transcriptome, genetic aberrations, and clinical data of WNT, SHH, Group 3, and Group 4 medulloblastomas. *Acta Neuropathol.* 2012; 123:473–484. [PubMed: 22358457]
10. Pugh TJ, Weeraratne SD, Archer TC, Pomeranz Krummel DA, Auclair D, Bochicchio J, et al. Medulloblastoma exome sequencing uncovers subtype-specific somatic mutations. *Nature.* 2012; 488:106–110. [PubMed: 22820256]
11. Ellison DW, Kocak M, Dalton J, Megahed H, Lusher ME, Ryan SL, et al. Definition of disease-risk stratification groups in childhood medulloblastoma using combined clinical, pathologic, and molecular variables. *J Clin Oncol.* 2011; 29:1400–1407. [PubMed: 20921458]
12. Northcott PA, Korshunov A, Witt H, Hielscher T, Eberhart CG, Mack S, et al. Medulloblastoma comprises four distinct molecular variants. *J Clin Oncol.* 2011; 29:1408–1414. [PubMed: 20823417]
13. Ellison DW, Dalton J, Kocak M, Nicholson SL, Fraga C, Neale G, et al. Medulloblastoma: clinicopathological correlates of SHH, WNT, and non-SHH/WNT molecular subgroups. *Acta Neuropathol.* 2011; 121:381–396. [PubMed: 21267586]
14. Gessi M, von Bueren AO, Rutkowski S, Pietsch T. p53 expression predicts dismal outcome for medulloblastoma patients with metastatic disease. *J Neurooncol.* 2011; 106:135–141. [PubMed: 21796446]
15. Sengupta R, Dubuc A, Ward S, Yang L, Northcott P, Woerner BM, et al. CXCR4 activation defines a new subgroup of Sonic hedgehog-driven medulloblastoma. *Cancer Res.* 2012; 72:122–132. [PubMed: 22052462]
16. Yauch RL, Dijkgraaf GJ, Aliche B, Januario T, Ahn CP, Holcomb T, et al. Smoothed mutation confers resistance to a Hedgehog pathway inhibitor in medulloblastoma. *Science.* 2009; 326:572–574. [PubMed: 19726788]
17. Gajjar AJ, Stewart CF, Ellison DW, Curran T, Phillips P, Goldman S, et al. A phase I pharmacokinetic trial of sonic hedgehog (SHH) antagonist GDC-0449 in pediatric patients with recurrent of refractory medulloblastoma: A Pediatric Brain Tumor Consortium study (PBTC 25). *J Clin Oncol.* 2010; 28(suppl; abstr CRA9501):18s.
18. Northcott PA, Shih DJ, Peacock J, Garzia L, Morrissy AS, Zichner T, et al. Subgroup-specific structural variation across 1,000 medulloblastoma genomes. *Nature.* 2012; 488:49–56. [PubMed: 22832581]
19. Cho YJ, Tsherniak A, Tamayo P, Santagata S, Ligon A, Greulich H, et al. Integrative genomic analysis of medulloblastoma identifies a molecular subgroup that drives poor clinical outcome. *J Clin Oncol.* 2011; 29:1424–1430. [PubMed: 21098324]
20. Kool M, Koster J, Bunt J, Hasselt NE, Lakeman A, van Sluis P, et al. Integrated genomics identifies five medulloblastoma subtypes with distinct genetic profiles, pathway signatures and clinicopathological features. *PLoS ONE.* 2008; 3:e3088. [PubMed: 18769486]
21. Bulavin DV, Demidov ON, Saito S, Kauraniemi P, Phillips C, Amundson SA, et al. Amplification of PPM1D in human tumors abrogates p53 tumor-suppressor activity. *Nat Genet.* 2002; 31:210–215. [PubMed: 12021785]
22. Nannenga B, Lu X, Dumble M, Van Maanen M, Nguyen TA, Sutton R, et al. Augmented cancer resistance and DNA damage response phenotypes in PPM1D null mice. *Mol Carcinog.* 2006; 45:594–604. [PubMed: 16652371]
23. Li J, Yang Y, Peng Y, Austin RJ, van Eyndhoven WG, Nguyen KC, et al. Oncogenic properties of PPM1D located within a breast cancer amplification epicenter at 17q23. *Nat Genet.* 2002; 31:133–134. [PubMed: 12021784]

24. Saito-Ohara F, Imoto I, Inoue J, Hosoi H, Nakagawara A, Sugimoto T, et al. PPM1D is a potential target for 17q gain in neuroblastoma. *Cancer Res.* 2003; 63:1876–1883. [PubMed: 12702577]
25. Castellino RC, De Bortoli M, Lu X, Moon SH, Nguyen TA, Shepard MA, et al. Medulloblastomas overexpress the p53-inactivating oncogene WIP1/PPM1D. *J Neurooncol.* 2008; 86:245–256. [PubMed: 17932621]
26. Mendrzyk F, Radlwimmer B, Joos S, Kokocinski F, Benner A, Stange DE, et al. Genomic and protein expression profiling identifies CDK6 as novel independent prognostic marker in medulloblastoma. *J Clin Oncol.* 2005; 23:8853–8862. [PubMed: 16314645]
27. Buss MC, Read TA, Schniederjan MJ, Gandhi K, Castellino RC. HDM2 promotes WIP1-mediated medulloblastoma growth. *Neuro Oncol.* 2012; 14:440–458. [PubMed: 22379189]
28. Remke M, Hielscher T, Northcott PA, Witt H, Ryzhova M, Wittmann A, et al. Adult medulloblastoma comprises three major molecular variants. *J Clin Oncol.* 2011; 29:2717–2723. [PubMed: 21632505]
29. Siu IM, Lal A, Blankenship JR, Aldosari N, Riggins GJ. c-Myc promoter activation in medulloblastoma. *Cancer Res.* 2003; 63:4773–4776. [PubMed: 12941792]
30. Pfister S. Medulloblastoma: a potpourri of distinct entities. *Acta Neuropathol.* 2012; 123:463–464. [PubMed: 22392443]
31. Rubin JB, Kung AL, Klein RS, Chan JA, Sun Y, Schmidt K, et al. A small-molecule antagonist of CXCR4 inhibits intracranial growth of primary brain tumors. *Proc Natl Acad Sci U S A.* 2003; 100:13513–13518. [PubMed: 14595012]
32. Woerner BM, Warrington NM, Kung AL, Perry A, Rubin JB. Widespread CXCR4 activation in astrocytomas revealed by phospho-CXCR4-specific antibodies. *Cancer Res.* 2005; 65:11392–11399. [PubMed: 16357147]
33. Vassilev LT, Vu BT, Graves B, et al. In vivo activation of the p53 pathway by small-molecule antagonists of MDM2. *Science.* 2004; 303:844–848. [PubMed: 14704432]
34. Shangary S, Wang S. Small-molecule inhibitors of the MDM2-p53 protein-protein interaction to reactivate p53 function: a novel approach for cancer therapy. *Annu Rev Pharmacol Toxicol.* 2009; 49:223–241. [PubMed: 18834305]
35. Issaeva N, Bozko P, Enge M, et al. Small molecule RITA binds to p53, blocks p53-HDM-2 interaction and activates p53 function in tumors. *Nat Med.* 2004; 10:1321–1328. [PubMed: 15558054]
36. Grinkevich VV, Nikulenkov F, Shi Y, et al. Ablation of key oncogenic pathways by RITA-reactivated p53 is required for efficient apoptosis. *Cancer Cell.* 2009; 15:441–453. [PubMed: 19411072]
37. Wang Z, Sun Y. Targeting p53 for Novel Anticancer Therapy. *Transl Oncol.* 2010; 3:1–12. [PubMed: 20165689]
38. Wu X, Northcott PA, Dubuc A, Dupuy AJ, Shih DJ, Witt H, et al. Clonal selection drives genetic divergence of metastatic medulloblastoma. *Nature.* 2012; 482:529–533. [PubMed: 22343890]
39. Barker BL, Benovic JL. G protein-coupled receptor kinase 5 phosphorylation of hip regulates internalization of the chemokine receptor CXCR4. *Biochemistry.* 2011; 50:6933–6941. [PubMed: 21728385]
40. Pfister S, Remke M, Benner A, Mendrzyk F, Toedt G, Felsberg J, et al. Outcome prediction in pediatric medulloblastoma based on DNA copy-number aberrations of chromosomes 6q and 17q and the MYC and MYCN loci. *J Clin Oncol.* 2009; 27:1627–1636. [PubMed: 19255330]
41. Clifford SC, Lusher ME, Lindsey JC, Langdon JA, Gilbertson RJ, Straughton D, et al. Wnt/Wingless pathway activation and chromosome 6 loss characterize a distinct molecular sub-group of medulloblastomas associated with a favorable prognosis. *Cell Cycle.* 2006; 5:2666–2670. [PubMed: 17172831]
42. Lamont JM, McManamy CS, Pearson AD, Clifford SC, Ellison DW. Combined histopathological and molecular cytogenetic stratification of medulloblastoma patients. *Clin Cancer Res.* 2004; 10:5482–5493. [PubMed: 15328187]
43. Pan E, Pellarin M, Holmes E, Smirnov I, Misra A, Eberhart CG, et al. Isochromosome 17q is a negative prognostic factor in poor-risk childhood medulloblastoma patients. *Clin Cancer Res.* 2005; 11:4733–4740. [PubMed: 16000568]

44. Traenka C, Remke M, Korshunov A, Bender S, Hielscher T, Northcott PA, et al. Role of LIM and SH3 protein 1 (LASP1) in the metastatic dissemination of medulloblastoma. *Cancer Res.* 2010; 70:8003–8014. [PubMed: 20924110]
45. Fiscella M, Zhang H, Fan S, Sakaguchi K, Shen S, Mercer WE, et al. Wip1, a novel human protein phosphatase that is induced in response to ionizing radiation in a p53-dependent manner. *Proc Natl Acad Sci U S A.* 1997; 94:6048–6053. [PubMed: 9177166]
46. Takekawa M, Adachi M, Nakahata A, Nakayama I, Itoh F, Tsukuda H, et al. p53-inducible wip1 phosphatase mediates a negative feedback regulation of p38 MAPK-p53 signaling in response to UV radiation. *Embo J.* 2000; 19:6517–526. [PubMed: 11101524]
47. Lu X, Ma O, Nguyen TA, Jones SN, Oren M, Donehower LA. The Wip1 Phosphatase acts as a gatekeeper in the p53-Mdm2 autoregulatory loop. *Cancer Cell.* 2007; 12:342–354. [PubMed: 17936559]
48. Shreeram S, Demidov ON, Hee WK, Yamaguchi H, Onishi N, Kek C, et al. Wip1 phosphatase modulates ATM-dependent signaling pathways. *Mol Cell.* 2006; 23:757–764. [PubMed: 16949371]
49. Lu X, Nannenga B, Donehower LA. PPM1D dephosphorylates Chk1 and p53 and abrogates cell cycle checkpoints. *Genes Dev.* 2005; 19:1162–1174. [PubMed: 15870257]
50. Fujimoto H, Onishi N, Kato N, Takekawa M, Xu XZ, Kosugi A, et al. Regulation of the antioncogenic Chk2 kinase by the oncogenic Wip1 phosphatase. *Cell Death Differ.* 2006; 13:1170–1180. [PubMed: 16311512]
51. Yoda A, Xu XZ, Onishi N, Toyoshima K, Fujimoto H, Kato N, et al. Intrinsic kinase activity and SQ/TQ domain of Chk2 kinase as well as N-terminal domain of Wip1 phosphatase are required for regulation of Chk2 by Wip1. *J Biol Chem.* 2006; 281:24847–24862. [PubMed: 16798742]
52. Demidov ON, Timofeev O, Lwin HN, Kek C, Appella E, Bulavin DV. Wip1 phosphatase regulates p53-dependent apoptosis of stem cells and tumorigenesis in the mouse intestine. *Cell Stem Cell.* 2007; 1:180–190. [PubMed: 18371349]
53. Pandolfi S, Montagnani V, Penachioni JY, Vinci MC, Olivito B, Borgognoni L, et al. WIP1 phosphatase modulates the Hedgehog signaling by enhancing GLI1 function. *Oncogene.* 2012 e-pub ahead of print 12 November 2012. 10.1038/onc.2012.502
54. Demidov ON, Kek C, Shreeram S, Timofeev O, Fornace AJ, Appella E, et al. The role of the MKK6/p38 MAPK pathway in Wip1-dependent regulation of ErbB2-driven mammary gland tumorigenesis. *Oncogene.* 2007; 26:2502–2506. [PubMed: 17016428]
55. Kleiblova P, Shaltiel IA, Benada J, Sevcik J, Pechackova S, Pohlreich P, et al. Gain-of-function mutations of PPM1D/Wip1 impair the p53-dependent G1 checkpoint. *J Cell Biol.* 2013; 201:511–521. [PubMed: 23649806]
56. Dudgeon C, Shreeram S, Tanoue K, Mazur SJ, Sayadi A, Robinson RC, et al. Genetic variants and mutations of PPM1D control the response to DNA damage. *Cell Cycle.* 2013; 12:2656–2664. [PubMed: 23907125]
57. Ruark E, Snape K, Humburg P, Loveday C, Bajrami I, Brough R, et al. Mosaic PPM1D mutations are associated with predisposition to breast and ovarian cancer. *Nature.* 2013; 493:406–410. [PubMed: 23242139]
58. Dorsam RT, Gutkind JS. G-protein-coupled receptors and cancer. *Nat Rev Cancer.* 2007; 7:79–94. [PubMed: 17251915]
59. Klein RS, Rubin JB, Gibson HD, DeHaan EN, Alvarez-Hernandez X, Segal RA, et al. SDF-1 alpha induces chemotaxis and enhances Sonic hedgehog-induced proliferation of cerebellar granule cells. *Development.* 2001; 128:1971–1981. [PubMed: 11493520]
60. Domanska UM, Kruijzinga RC, Nagengast WB, Timmer-Bosscha H, Huls G, de Vries EG, et al. A review on CXCR4/CXCL12 axis in oncology: No place to hide. *Eur J Cancer.* 2013; 49:219–230. [PubMed: 22683307]
61. Bian XW, Yang SX, Chen JH, Ping YF, Zhou XD, Wang QL, et al. Preferential expression of chemokine receptor CXCR4 by highly malignant human gliomas and its association with poor patient survival. *Neurosurgery.* 2007; 61:570–578. discussion 578-579. [PubMed: 17881971]

62. Calatuzzolo C, Maderna E, Pollo B, Gelati M, Marras C, Silvani A, et al. Prognostic value of CXCL12 expression in 40 low-grade oligodendrogliomas and oligoastrocytomas. *Cancer Biol Ther.* 2006; 5:827–832. [PubMed: 16760646]
63. Krupnick JG, Benovic JL. The role of receptor kinases and arrestins in G protein-coupled receptor regulation. *Annu Rev Pharmacol Toxicol.* 1998; 38:289–319. [PubMed: 9597157]
64. Orsini MJ, Parent JL, Mundell SJ, Marchese A, Benovic JL. Trafficking of the HIV coreceptor CXCR4. Role of arrestins and identification of residues in the c-terminal tail that mediate receptor internalization. *J Biol Chem.* 1999; 274:31076–31086. [PubMed: 10521508]
65. Goodrich LV, Milenkovic L, Higgins KM, Scott MP. Altered neural cell fates and medulloblastoma in mouse patched mutants. *Science.* 1997; 277:1109–1113. [PubMed: 9262482]
66. Rao G, Pedone CA, Coffin CM, Holland EC, Fults DW. c-Myc enhances sonic hedgehog-induced medulloblastoma formation from nestin-expressing neural progenitors in mice. *Neoplasia.* 2003; 5:198–204. [PubMed: 12869303]
67. Mumert M, Dubuc A, Wu X, Northcott PA, Chin SS, Pedone CA, et al. Functional genomics identifies drivers of medulloblastoma dissemination. *Cancer Res.* 2012; 72:4944–4953. [PubMed: 22875024]
68. Remke M, Hielscher T, Korshunov A, Northcott PA, Bender S, Kool M, et al. FSTL5 is a marker of poor prognosis in non-WNT/non-SHH medulloblastoma. *J Clin Oncol.* 2011; 29:3852–3861. [PubMed: 21911727]
69. Castellino RC, De Bortoli M, Lin LL, Skapura DG, Rajan JA, Adesina AM, et al. Overexpressed TP73 induces apoptosis in medulloblastoma. *BMC Cancer.* 2007; 7:127. [PubMed: 17626635]

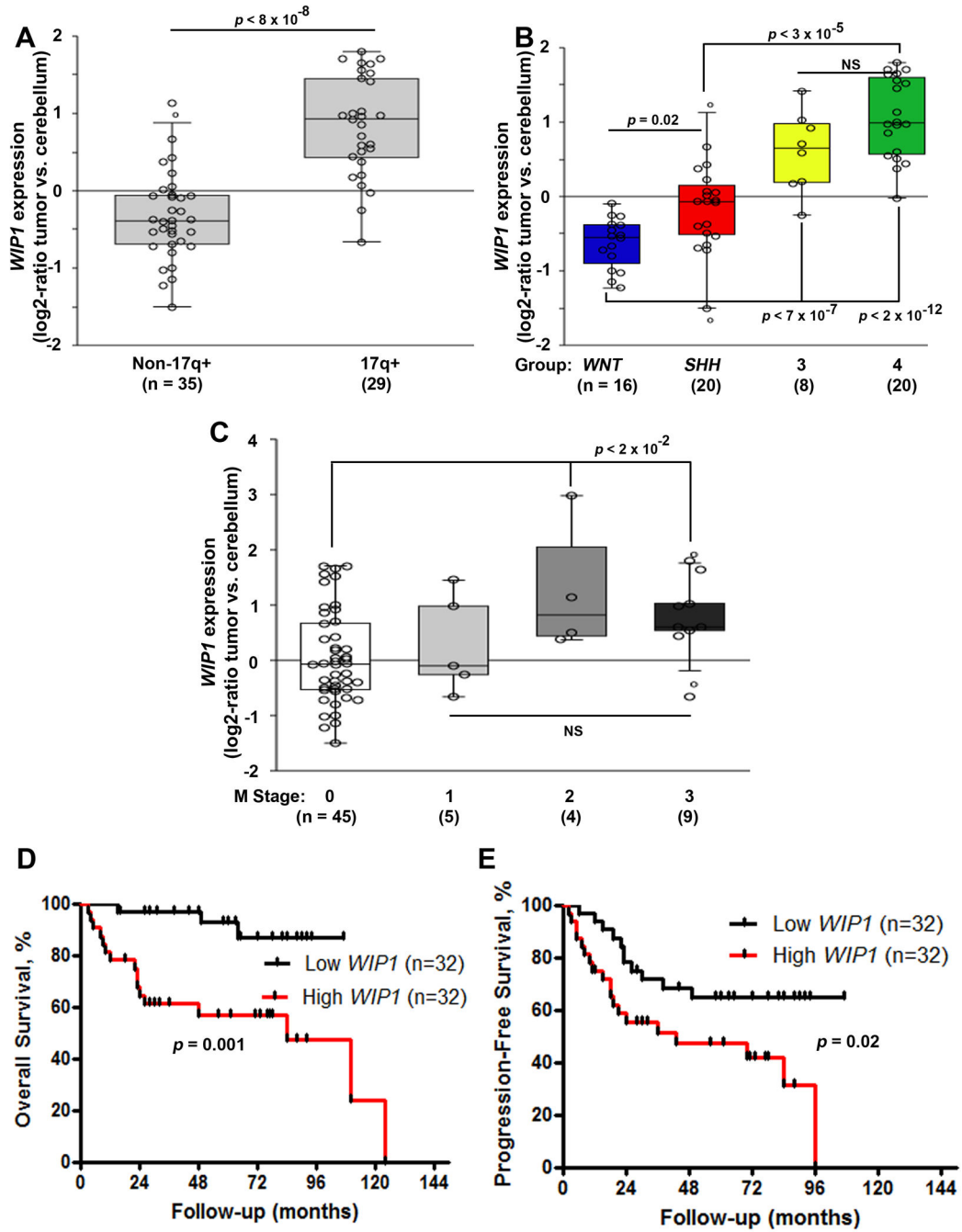


Figure 1. High *WIP1* expression in medulloblastoma is associated with adverse prognostic factors and inferior survival

(A) *WIP1* expression, based on gene expression profiling, in 64 pediatric medulloblastomas, with or without gain of chromosome 17q. Copy number status of chromosome 17q was determined using an Agilent-014850 Whole Human Genome Microarray 4×44K G4112F and array-based comparative genomic hybridization (CGH). (B) *WIP1* expression among medulloblastoma subgroups. Subgroup affiliation was determined using unsupervised clustering approaches. (C) *WIP1* expression, segregated by Chang M stage. R2 software was

used to compare *WIP1* expression according to 17q status, subgroup, and M stage. **(D, E)** Kaplan-Meier analysis of patient survival was based on median *WIP1* expression. Survival was measured from diagnosis until death or last follow-up. Patient survival was analyzed according to the Kaplan-Meier method, using log-rank statistics. The median value, in panels A-C, is denoted by the middle line in each rectangle. Whiskers represent the bottom 10th and top 90th percentiles. The Y-axis denotes relative expression (log₂-ratio tumor vs. cerebellum controls). NS, not significant.

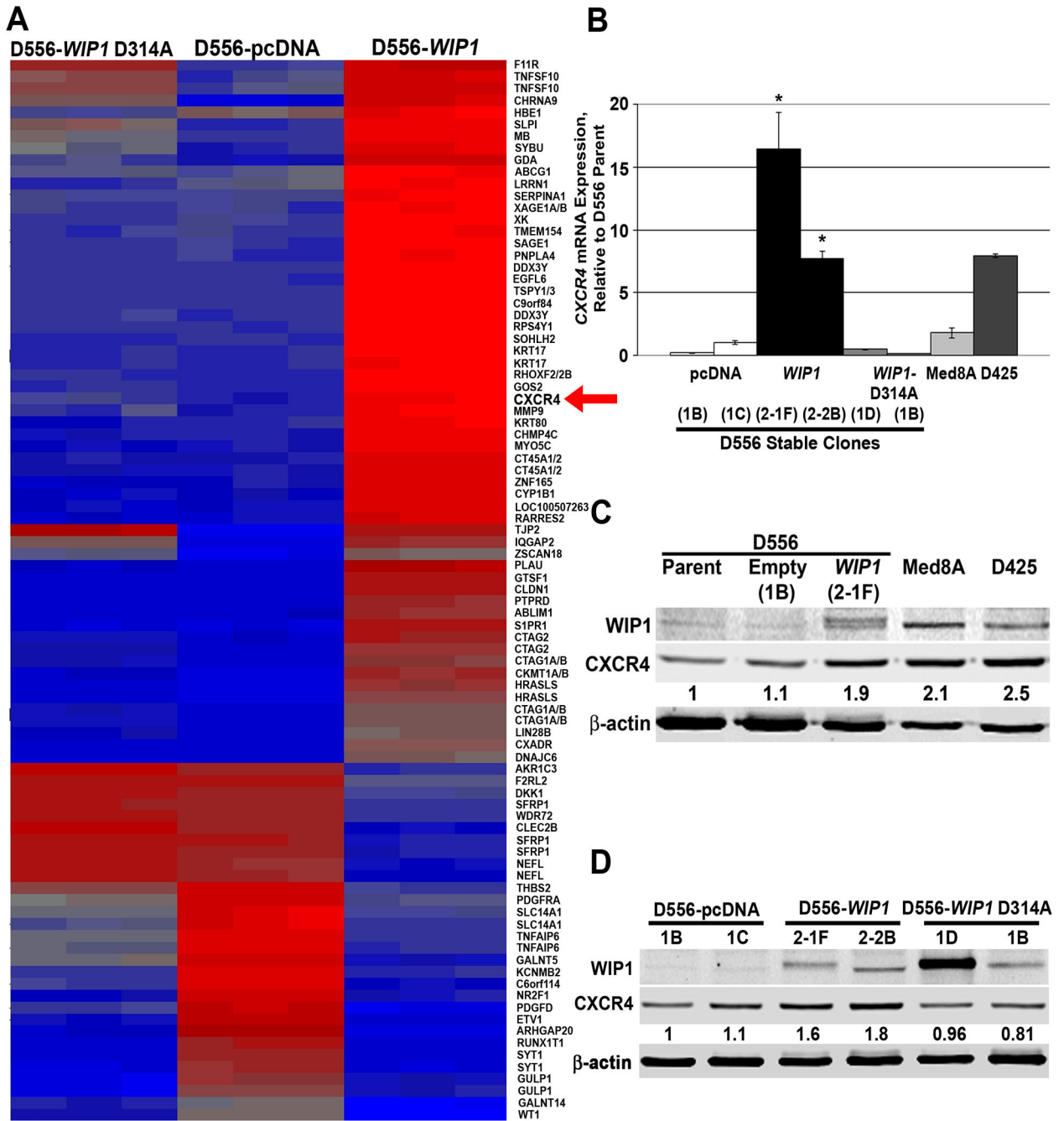


Figure 2. Association of WIP1 and CXCR4 expression in medulloblastoma cells

(A) Heat map of gene expression in D56 cells with stable expression of empty vector (pcDNA3), WIP1 (D56-WIP1), or mutant, phosphatase-dead WIP1 (WIP1 D314A). Three clones from D56 stable cell lines were run in triplicate on an Affymetrix HG-U133 Plus 2.0 Array. Data were normalized using the Robust MultiChip Average algorithm. Differential gene analysis was performed using an ANOVA model, with an absolute fold change threshold of 6 and a p-value with an FDR threshold of 0.001. Up-regulated genes are shown in red (red arrow, CXCR4); down-regulated genes in blue. (B) CXCR4 mRNA expression by

real-time, RT-PCR. Absolute gene expression was determined based on standard curves. Target gene expression was normalized to *GAPDH* expression. (C, D) Western blotting confirmed increased expression of CXCR4 protein in *WIP1* high-expressing medulloblastoma cell lines. CXCR4 protein expression was quantified from near-infrared fluorescence and normalized to expression of β -actin, the loading control. The relative amount of CXCR4 (noted below each western blot for CXCR4) is expressed as a ratio of normalized CXCR4 expression in a particular lane, to normalized expression of CXCR4 in (C) D556 parental or (D) D556-pcDNA stable cells. Error bars, standard error of the mean. Experiments were repeated at least three times.

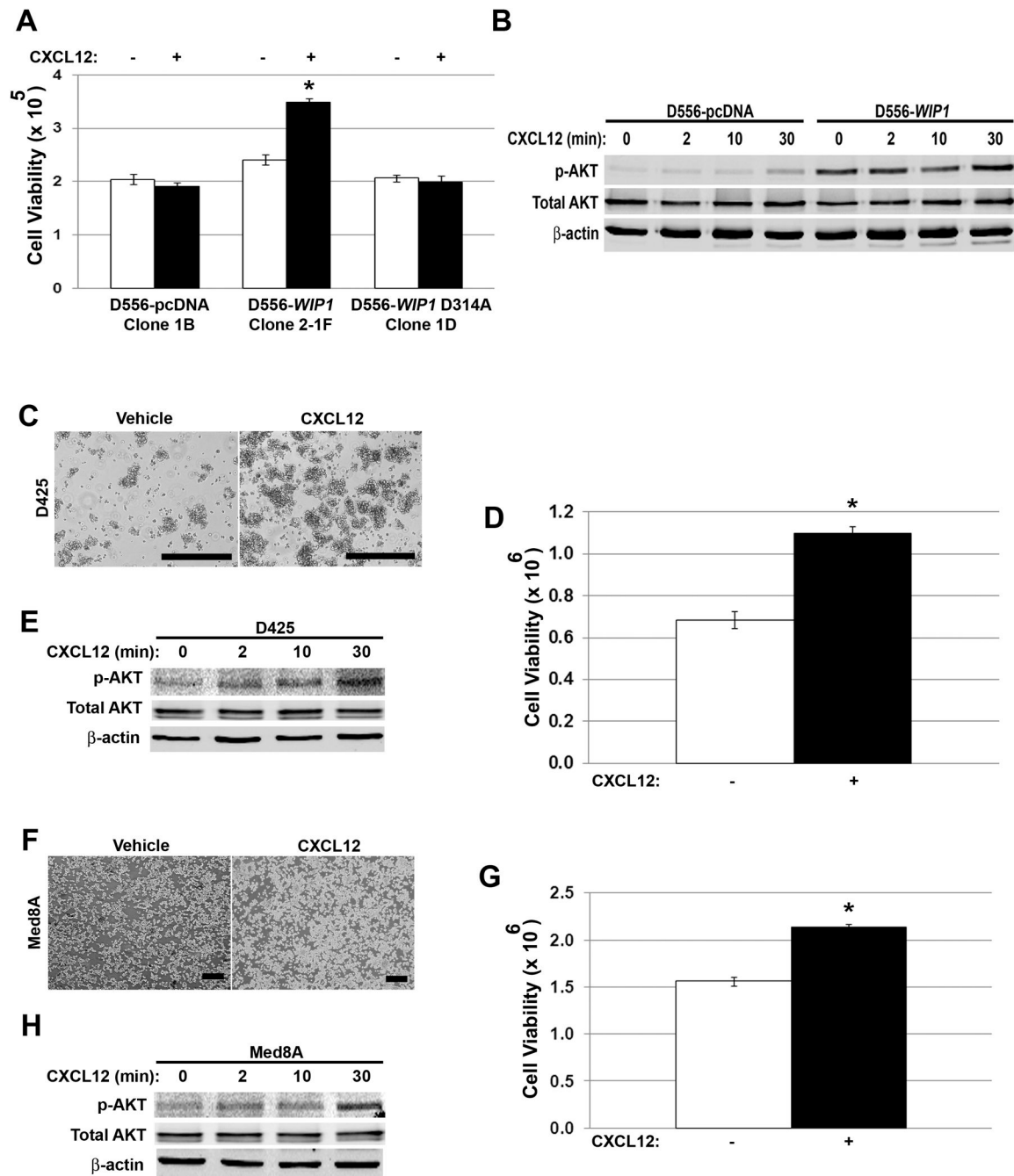


Figure 3. Stimulation with SDF1 α activates PI-3 kinase signaling and promotes growth of WIP1 high-expressing medulloblastoma cells

(A) Number of viable D556 stably-transfected cells by trypan blue exclusion (i.e. viability; Y-axis), 48 hours following serum starvation and stimulation with vehicle (-) or CXCL12 (+; SDF1 α , 1 μ g/mL). *, $p < 0.0002$. (B) Western blotting of whole cell lysates from (A) for Ser473-phosphorylated and total AKT. (C, F) Photomicrographs and (D, G) number of viable D425 and Med8A cells by trypan blue exclusion, respectively, 48 hours following serum starvation and SDF1 α stimulation, as above. Scale bars, 400 μ m. *, $p < 0.0002$. (E, H) Western blotting of whole cell lysates from (C, F) for Ser473-phosphorylated and total AKT.

H) Western blotting of whole cell lysates from **(D, G)** for serine 473-phosphorylated and total AKT. Error bars, standard deviation. Experiments were repeated at least three times.

Author Manuscript

Author Manuscript

Author Manuscript

Author Manuscript

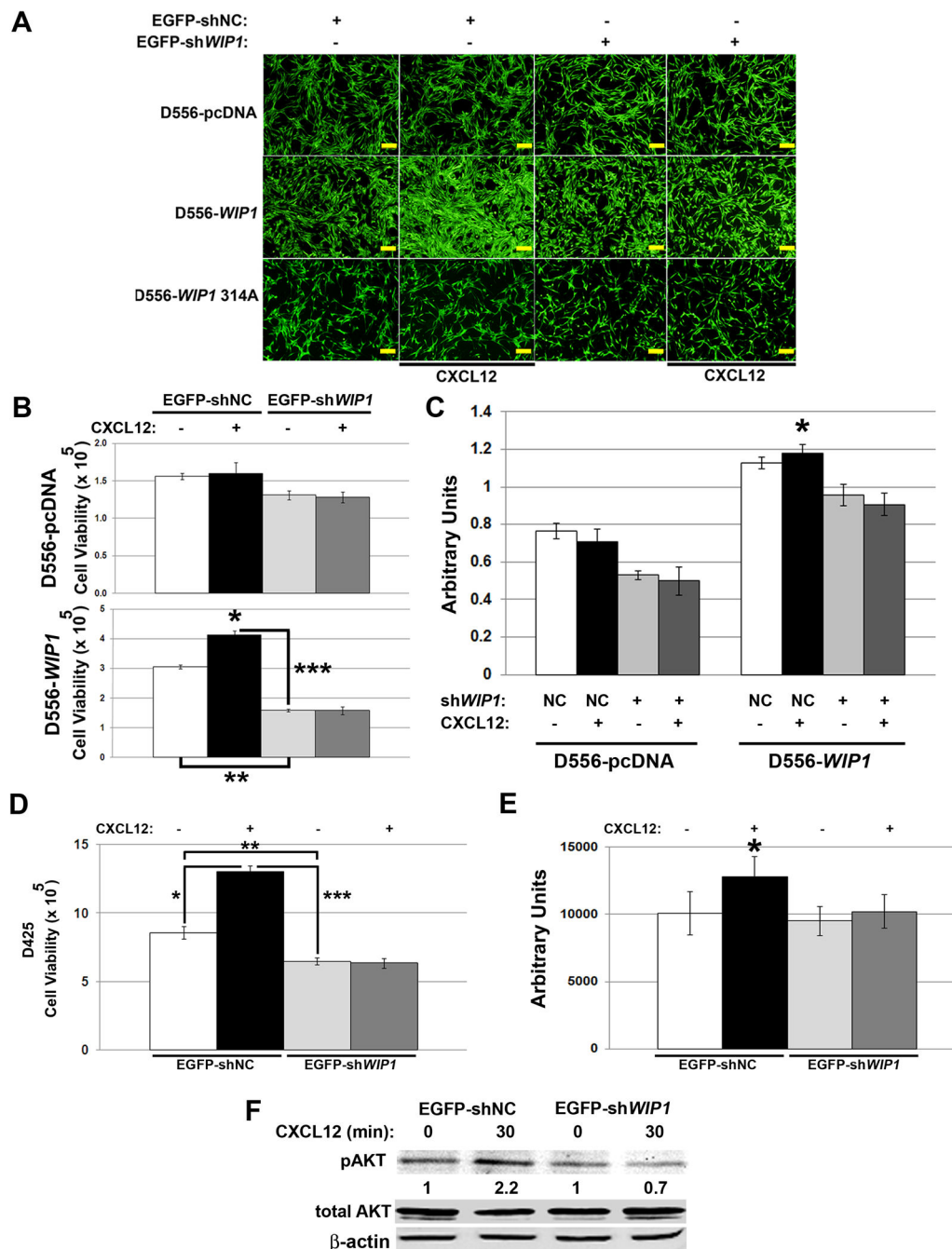


Figure 4. WIP1 knock-down suppresses SDF1 α -stimulated growth of WIP1 high-expressing medulloblastoma cells

(A) Representative photomicrographs of enhanced green fluorescent protein (EGFP) fluorescence, (B) number of viable cells by trypan blue exclusion (Y-axis), and (C) proliferation, as measured by absorbance following incubation with WST-1 reagent, of D556 stably-transfected cells in serum-free media 48 hours following infection with EGFP-tagged negative control (EGFP-shNC; NC) or WIP1 shRNA-encoding (EGFP-shWIP1) lentivirus, and stimulation with vehicle (-) or CXCL12 (+; SDF1 α , 1 μ g/mL) for 48 hours.

Scale bars, 500 μm . *, $p < 0.003$; **, $p < 0.00001$; ***, $p < 0.00003$. **(D)** Number of viable D425 cells by trypan blue exclusion and **(E)** proliferation, as measured by assayed by luminescence following incubation with CellTiter-Glo® reagent, following infection with EGFP-shNC or -shWIP1 lentivirus, and stimulation with vehicle or SDF1 α for 48 hours. *, $p < 0.0003$; **, $p < 0.007$; ***, $p < 0.00004$. **(F)** Western blotting of whole cell lysates from **(D)**. Serine 473-phosphorylated AKT (pAKT) protein expression was quantified from near-infrared fluorescence and normalized to expression of β -actin, the loading control. The relative pAKT expression is shown as a ratio of normalized pAKT expression in SDF1 α -stimulated to unstimulated D425 cells. Experiments were repeated at least twice.

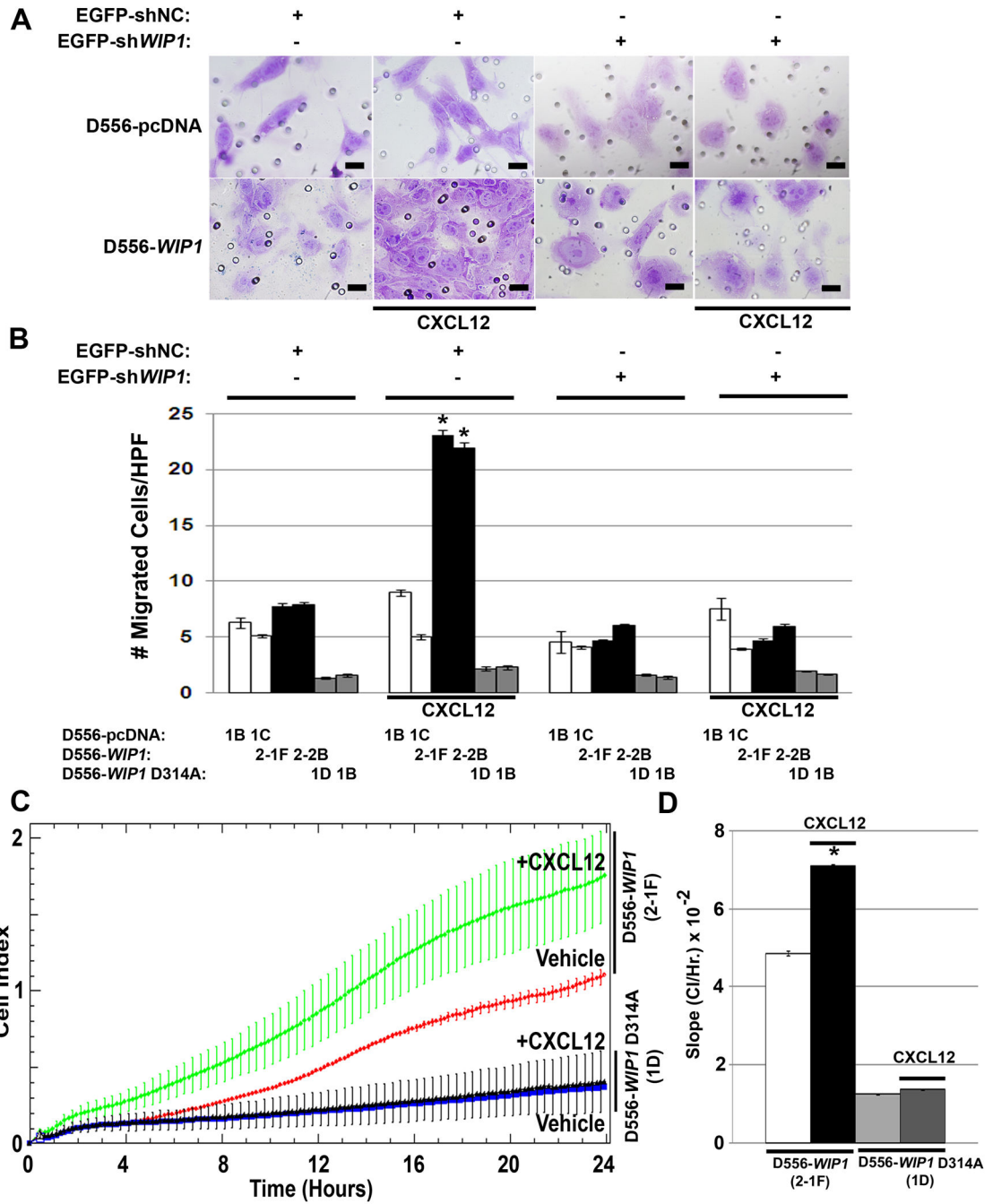


Figure 5. SDF1 α stimulation promotes invasion and migration of D556-WIP1 stable clones
 (A) Representative photomicrographs of D556-pcDNA and D556-WIP1 stable clones that have migrated through a Boyden Chamber 48 hours following infection with WIP1 shRNA or empty-vector-containing lentiviral particles, and stimulation with vehicle or CXCL12 (SDF1 α , 1 μ g/mL). Scale bars, 50 μ m. (B) Quantification of migrated D556 stable clones, as described in (A). Bar graphs represent the average number of migrated cells per high-power field (HPF) in triplicate measurements of 10 representative HPFs per treatment. Error bars, standard deviation. *, $p < 5 \times 10^{-22}$. (C) Invasion of D556-WIP1 or D556-WIP1 D314A

cells through pores of a CIM plate, as measured by Cell Index (CI, arbitrary units), in response to stimulation with vehicle or SDF1 α (1 μ g/mL). Error bars denote SD among replicates. **(D)** Bar graphs represent the average change in CI per hour for invading D556-*WIP1* or D556-*WIP1* D314A cells stimulated with vehicle or SDF1 α . Error bars denote SD among replicates of at least 3 per treatment and experiment. *, $p < 0.005$. Experiments in Panels **A-B** were repeated three times; those in Panels **C-D** were repeated twice.

Author Manuscript

Author Manuscript

Author Manuscript

Author Manuscript

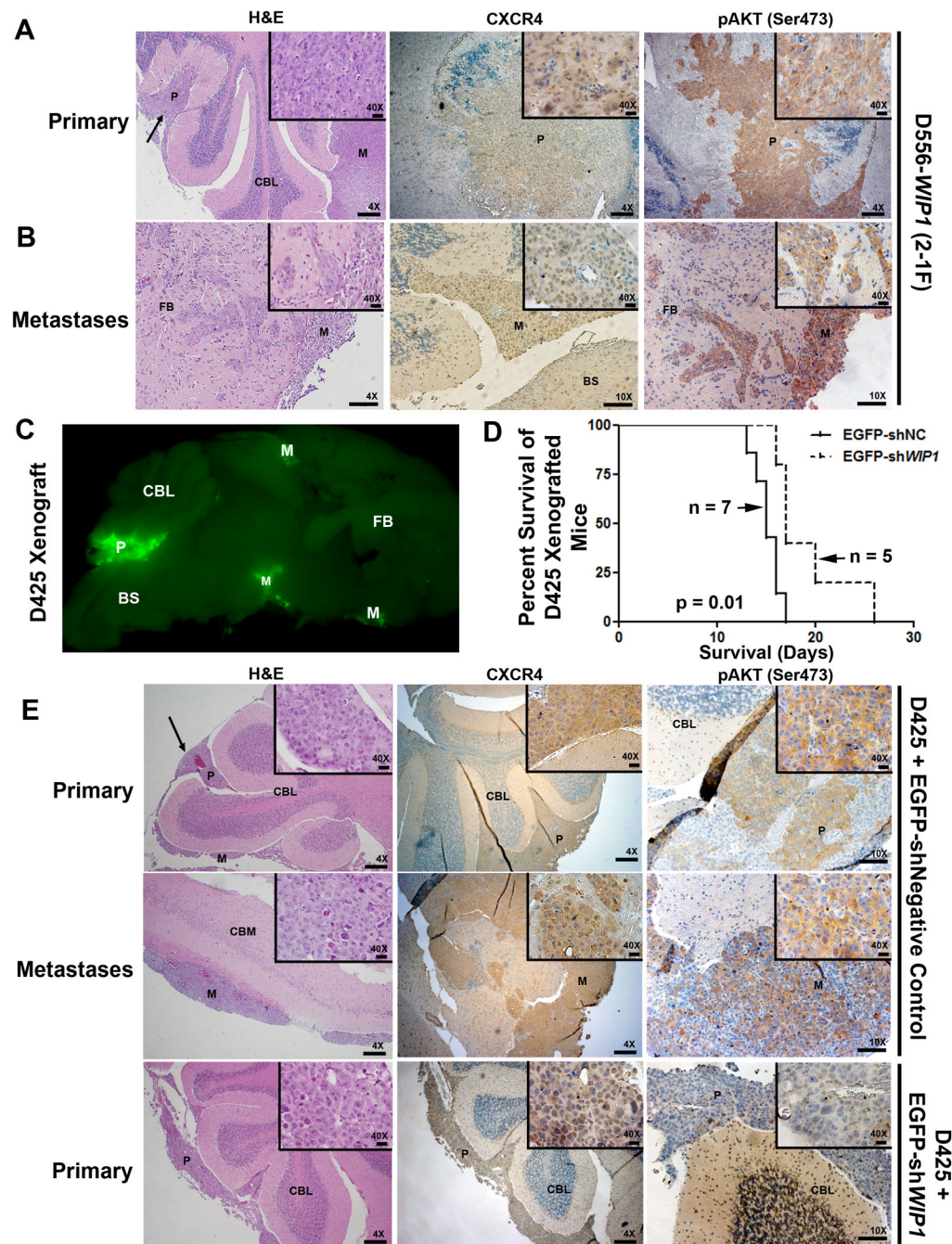


Figure 6. Primary and metastatic tumors from *WIP1*-expressing medulloblastoma xenografts express CXCR4

D556-*WIP1* (5×10^5) or D425 (1×10^6) cells were infected with lentiviral particles (multiplicity of infection, MOI = 2) containing control or *WIP1* shRNA. Twenty-four hours later, cells were harvested and injected into the cerebellum of SCID/Beige mice, 1mm posterior to the junction of the parietal and interparietal sutures, 1 mm lateral to midline, and at a 30° angle to the surface of the cerebellum, at a depth of 1 mm. Mice were sacrificed upon development of symptoms of medulloblastoma. Mouse brains were sectioned

sagittally, fixed in 4% formalin, and paraffin embedded for pathological examination. **(A)** Representative hematoxylin and eosin (H&E)-stained primary and **(B)** metastatic tumors from intracerebellar xenografts of D556-*WIP1* cells. IHC for CXCR4 and Ser473-phosphorylated AKT (pAKT) in primary and metastatic D556-*WIP1* tumors (n = 4). **(C)** Representative GFP fluorescence, prior to fixation, and **(D)** Kaplan-Meier survival of EGFP-shNC or EGFP-sh*WIP1*-infected D425 intracerebellar xenografted mice. **(E)** H&E and IHC of sagittally-sectioned mouse brains following orthotopic xenografting of EGFP-tagged lentivirus-infected D425 medulloblastoma cells. IHC for CXCR4 and pAKT in primary and metastatic D425 tumors (n = 4). BS, brain-stem; CBL, cerebellum; CBM, cerebrum; FB, forebrain; P, primary tumor; M, metastasis. Magnification 4×; Scale bars, 200 μm. Magnification 10×; Scale bars, 100 μm. Magnification 40×; Scale bars, 20 μm.

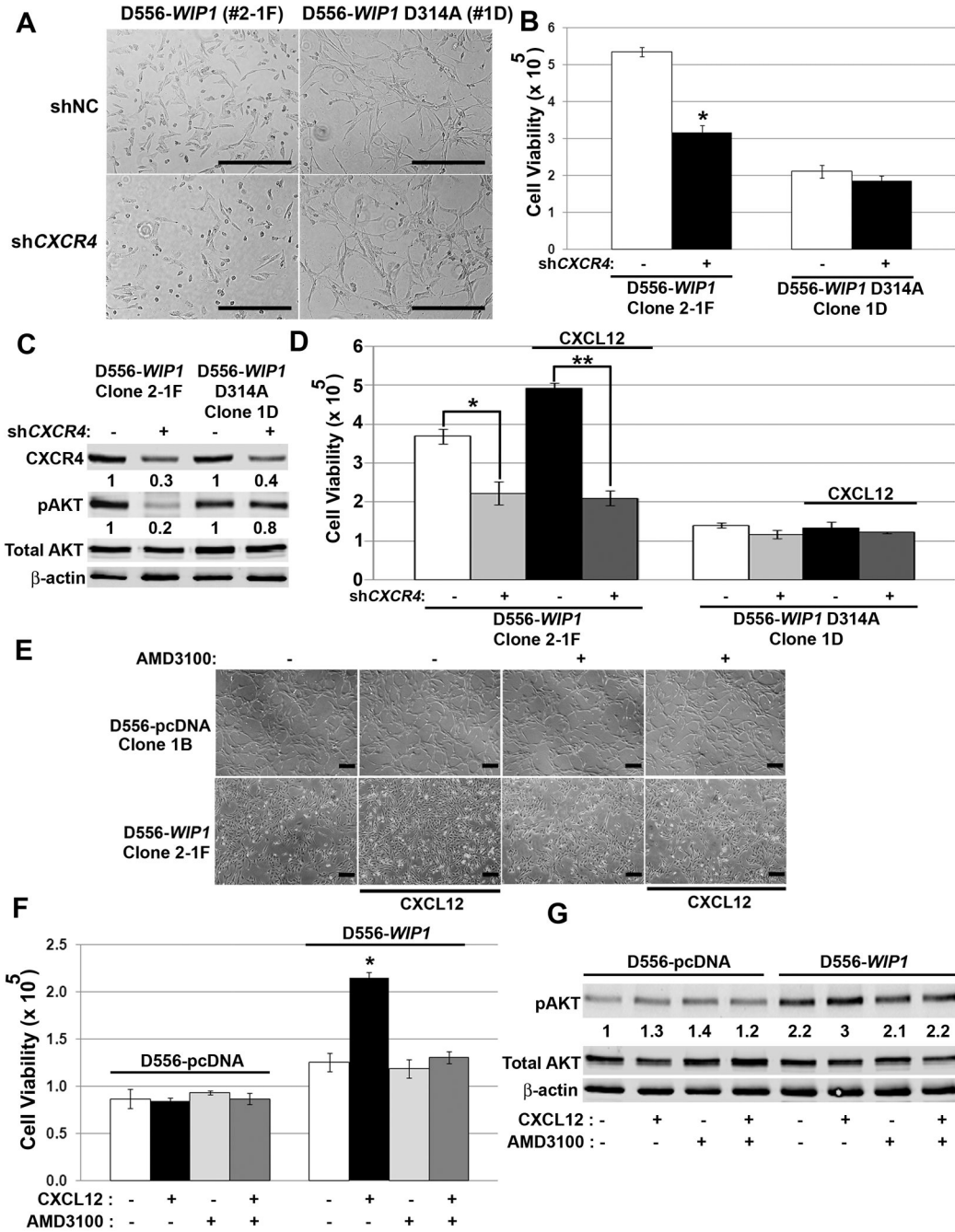


Figure 7. CXCR4 inhibition suppresses the growth of WIP1 high-expressing medulloblastoma cells

(A) Representative photomicrographs and (B) number of viable D556-WIP1 and D556-WIP1 D314A cells (Y-axis) in serum-containing media, by trypan blue exclusion, 72 hours following lentiviral-mediated CXCR4 knock-down. *, $p < 0.0005$. (C) Western blotting of whole cell lysates from (B) for CXCR4, Ser473 phosphorylated-, and total AKT, 72 hours following lentiviral-mediated CXCR4 knock-down. CXCR4 and Ser473-phosphorylated AKT (pAKT) protein expression was quantified from near-infrared fluorescence and

normalized to expression of β -actin. The relative amount of protein in either cell clone is expressed as a ratio of normalized CXCR4 or pAKT, to normalized expression following infection with control shRNA-containing lentivirus. **(D)** Number of viable cells (Y-axis) in serum-free media 72 hours following lentiviral-mediated knock-down of *CXCR4*, and stimulation with either vehicle or CXCL12 (SDF1 α , 1 μ g/mL). *, $p < 0.005$; **, $p < 0.0001$. **(E)** Representative photomicrographs and **(F)** number of viable (Y-axis) D556-*WIP1* and D556-pcDNA cells in serum-free media 72 hours following stimulation with vehicle or CXCL12, and treatment with vehicle or 20 μ M AMD3100. *, $p < 0.0007$. **(G)** Western blotting of whole cell lysates, as described in **(F)**. Expression is quantified from near-infrared fluorescence, relative to expression in CXCL12-unstimulated, AMD3100-untreated D556-pcDNA cells, and normalized to β -actin. Scale bars, 400 μ m. Error bars, standard deviation. Experiments were repeated at least three times.

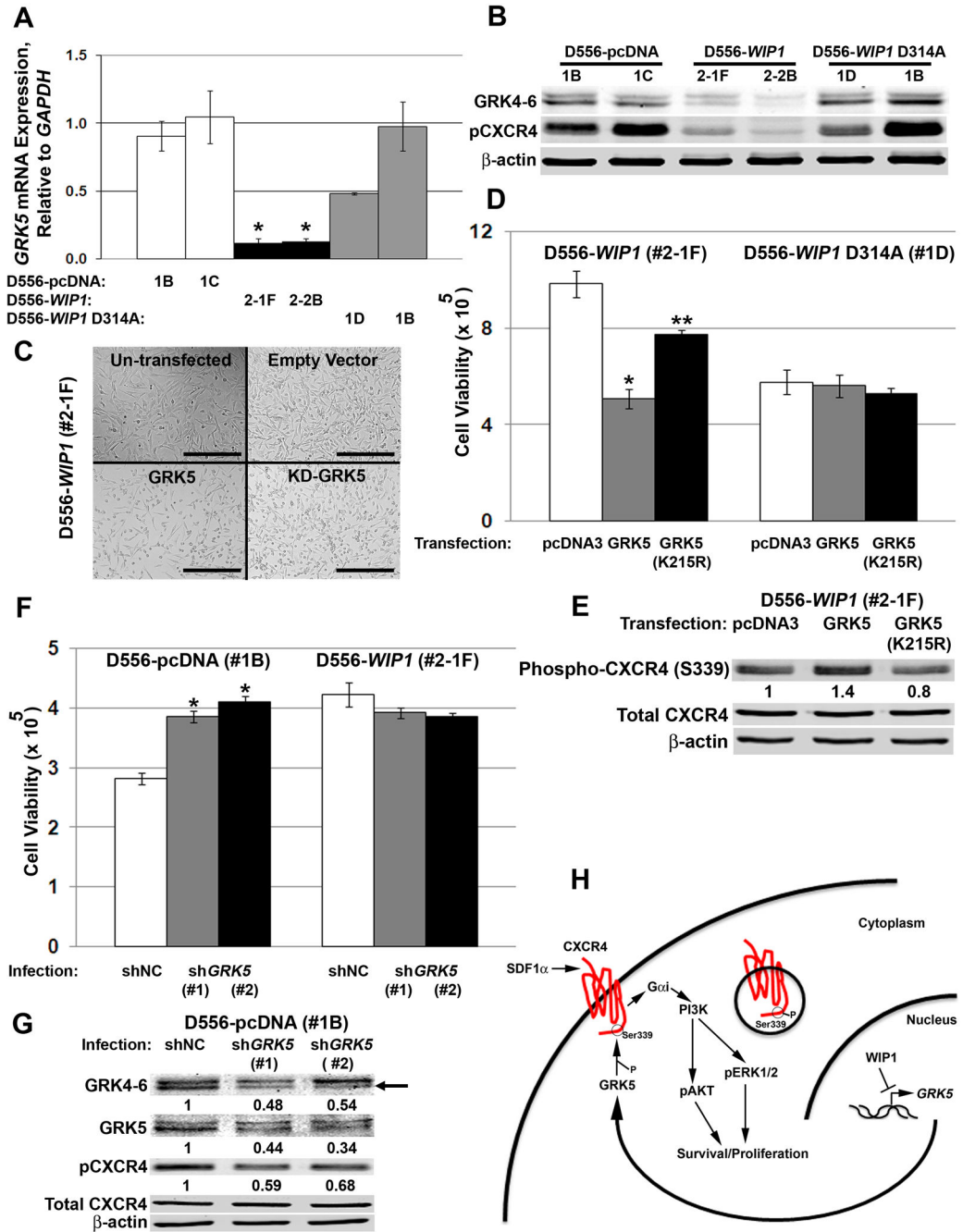


Figure 8. WIP1 promotes medulloblastoma growth by inhibiting Ser339 phosphorylation of CXCR4 through suppression of GRK5

(A) Real-time, RT-PCR for *GRK5*, relative to *GAPDH*, in D556 stable clones. *, $p < 0.0005$. Error bars, standard error of the mean. (B) Western blotting of whole cell lysates for GRK5, Ser339-phosphorylated CXCR4, and β-actin. The GRK4-6 antibody is specific for GRK4, GRK5, and GRK6. (C) Representative photomicrographs and (D) number of viable cells (Y-axis) by trypan blue exclusion following transfection with empty vector (pcDNA3), wild-type, or kinase-dead *GRK5* (KD-*GRK5*, *GRK5* K215R). *, $p < 0.0005$; **, $p < 0.02$. Error

bars, standard deviation (SD). (E) Western blotting of whole cell lysates following transfection, as in (D). Ser339-phosphorylated CXCR4 protein expression was quantified from near-infrared fluorescence and normalized to expression of β -actin. The relative amount of protein is expressed as a ratio of normalized Ser339-phosphorylated CXCR4, to normalized expression following transfection with an empty vector control (pcDNA3). (F) Number of viable cells (Y-axis), 48 hours following infection with negative control pLKO.1 or *GRK5* shRNA-containing lentivirus. *, $p < 0.0003$. Error bars, SD. (G) Western blotting of whole cell lysates, as in (F). *GRK5* is the lower band (black arrow). Protein expression was normalized to expression of β -actin, and shown relative to expression following transduction with an empty vector-containing shRNA lentivirus (shNC). (H) Model: *GRK5* promotes Ser339 phosphorylation and internalization of CXCR4. *WIP1* suppresses *GRK5* expression, which in turn permits membrane localization of CXCR4 and medulloblastoma growth and invasion in response to SDF1 α stimulation.

Table 1

Patient characteristics

	No. of patients	<i>WIP1</i> High	<i>WIP1</i> Low
Age (years)			
<3	3	2	1
3-18	37	20	17
>18	24	10	14
Gender			
Male	39	17	22
Female	25	15	10
Chang stage			
M0	45	18	28
M1	5	2	3
M2	4	4	0
M3	9	8	1
No information	1	0	0
Molecular subtype			
<i>WNT</i> -activated	16	0	16
<i>SHH</i> -activated	20	8	12
Group 3	8	7	1
Group 4	20	19	1
17q status			
Copy number gain	29	26	3
Total	64		

WIP1 high versus low expression is based on median *WIP1* expression. Age refers to age at diagnosis. Chang staging refers to published criteria for staging of medulloblastoma metastasis. Molecular subtyping was determined using unsupervised clustering approaches. Copy number status of 17q was determined using array-based comparative genomic hybridization. Abbreviations: *WNT*, wingless; *SHH*, sonic hedgehog; 17q, long arm of chromosome 17.

Table 2
D556 Medulloblastoma Xenograft IHC for Phospho-AKT (Ser473)

Xenografts	Phospho-AKT (Ser473) Intensity	Phospho-AKT (Ser473) Extent	Distant Mets	Local Mets	Invasion
D556-pcDNA (1B)					
#1	1+	5-10%	No	No	Yes
#2	1+	5-10%	No	No	No
#3	0	0%	No	No	No
#4	0	0%	No	No	No
D556-WIP1 (2-1F)					
#1	2-3+	Diffuse	No	Yes	Yes
#2	2-3+	Diffuse	No	Yes	Yes
#3	2-3+	Diffuse	Yes	Yes	Yes
#4	2+	Diffuse	No	Yes	Yes